




BRAIN COMMUNICATIONS

Network mediation of pathology pattern in sporadic Creutzfeldt–Jakob disease

 Benjamin Freeze,^{1,*}  Pedro Maia,²  Sneha Pandya¹ and Ashish Raj^{1,2}

*Present address: Department of Radiology, Massachusetts General Hospital, Harvard Medical School, 55 Fruit St., Boston, MA 02114, USA.

Sporadic Creutzfeldt–Jakob disease is a rare fatal rapidly progressive dementia caused by the accumulation and spread of pathologically misfolded prions. Evidence from animal models and *in vitro* experiments suggests that prion pathology propagates along neural connectivity pathways, with the transmission of misfolded prions initiating a corruptive templating process in newly encountered brain regions. Although particular regional patterns of disease have been recognized in humans, the underlying mechanistic basis of these patterns remains poorly understood. Here, we demonstrate that the spatial pattern of disease derived from publicly available human diffusion-weighted MRI data demonstrates stereotypical features across patient cohorts and can be largely explained by intrinsic connectivity properties of the human structural brain network. Regional diffusion-weighted MRI signal abnormalities are predicted by graph theoretical measures of centrality, with highly affected regions such as cingulate gyrus demonstrating strong structural connectivity to other brain regions. We employ network diffusion modelling to demonstrate that the spatial pattern of disease can be predicted by a diffusion process originating from a single regional pathology seed and operating on the structural connectome. The most likely seeds correspond to the most highly affected brain regions, suggesting that pathological prions could originate in a single brain region and spread throughout the brain to produce the regional distribution of pathology observed on MRI. Further investigation of top seed regions and associated connectivity pathways may be a useful strategy for developing therapeutic approaches.

1 Department of Radiology, NewYork-Presbyterian Hospital/Weill Cornell Medicine, New York, NY 10065, USA

2 Department of Radiology and Biomedical Imaging, University of California, San Francisco, San Francisco, CA 94143, USA

Correspondence to: Benjamin Freeze, MD, PhD, Department of Radiology
Massachusetts General Hospital, Harvard Medical School, 55 Fruit St., Boston, MA 02114, USA
E-mail: bfreeze@mgh.harvard.edu

Keywords: Creutzfeldt–Jakob disease; prion; MRI; structural connectivity; network diffusion

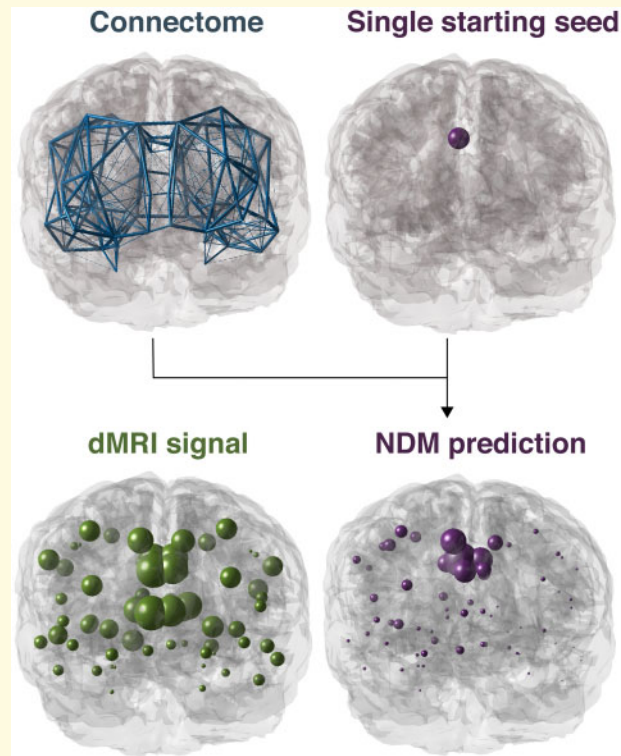
Abbreviations: ABA = Allen Brain Atlas; dMRI = diffusion-weighted MRI; GM = grey matter; NDM = network diffusion modelling; PrP^{Sc} = scrapie prion protein; sCJD = sporadic Creutzfeldt–Jakob disease; SR = seed region likelihood

Received August 5, 2019. Revised April 15, 2020. Accepted April 17, 2020. Advance Access publication May 15, 2020

© The Author(s) (2020). Published by Oxford University Press on behalf of the Guarantors of Brain.

This is an Open Access article distributed under the terms of the Creative Commons Attribution Non-Commercial License (<http://creativecommons.org/licenses/by-nc/4.0/>), which permits non-commercial re-use, distribution, and reproduction in any medium, provided the original work is properly cited. For commercial re-use, please contact journals.permissions@oup.com

Graphical Abstract



Introduction

Sporadic Creutzfeldt–Jakob disease (sCJD) is a fatal rapidly progressive dementia caused by the accumulation of misfolded pathological prion proteins [scrapie prion protein (PrP^{Sc})] throughout the brain. Prion deposition is accompanied by a number of pathological hallmarks including neuronal cell death, gliosis and spongiform change (Manners *et al.*, 2009). Because PrP^{Sc} is capable of inducing conformational conversion of normal cellular prion protein to PrP^{Sc} (Pan *et al.*, 1993), introduction of even a single PrP^{Sc} molecule may initiate a profound conversion of cellular prion protein into pathological species by positive feedback. Multiple lines of evidence suggest that PrP^{Sc} spreads along neural connectivity pathways (Fraser, 1982; Bartz *et al.*, 2003), suggesting that intrinsic properties of the brain structural connectome may influence the spatial patterning of disease. However, investigation of this hypothesis in humans has been limited by patient heterogeneity, small datasets and paucity of appropriate analytic techniques. As combined neuroimaging and computational modelling approaches have been successfully employed to explain disease patterning in neurodegenerative disorders such as Alzheimer’s disease (Raj *et al.*, 2012) and Parkinson’s disease (Pandya *et al.*, 2019), a similar approach may provide insight into the mechanisms controlling spatial patterning in sCJD.

In recent years, there has been recognition that diffusion-weighted MRI (dMRI) demonstrates marked abnormalities in sCJD (Shiga *et al.*, 2004; Young *et al.*, 2005) and is important for accurate imaging-based diagnosis of sCJD (Zerr *et al.*, 2009). Areas of dMRI abnormality have also been shown to correspond to pathological hallmarks, demonstrating that dMRI is an imaging biomarker of sCJD pathology (Manners *et al.*, 2009). Two studies are particularly notable for their relatively large number of CJD patients and high-quality dMRI data. Vitali *et al.* (2011) analyzed dMRI from 48 sCJD patients, and Eisenmenger *et al.* (2016) obtained data from 37 sCJD patients. These two groups used essentially the same regional brain parcellations and semi-quantitative scoring schemes to report dMRI findings. Here, we utilize regional dMRI data from these studies to investigate factors that may control or mediate regional vulnerability to sCJD pathology and its spatial patterning throughout the brain.

Using an analysis procedure that integrates regional dMRI of patients with the structural connectome of healthy subjects (which is used in the absence of an available CJD-specific connectome), we show that highly affected brain regions demonstrate elevated interregional connectivity, which may predispose to infection by propagating pathological prion species. We ask whether the spatial pattern of disease can be predicted from a disease

spread process from a single brain region. To this end, we employ network diffusion modelling (NDM) (Raj *et al.*, 2012), which mathematically encapsulates the spread of prions along neural connectivity pathways as a diffusion process on the structural connectome. It should be noted that this mathematically defined diffusion process is unrelated to dMRI, despite similar-sounding terminology. Furthermore, dMRI was used here to compute measures of the microstructural properties of grey matter (GM) structures under disease conditions, and not, as is typical in dMRI studies, as a means of computing the loss of structural integrity of white matter fibres. In this study, we do not consider whether and how white matter architecture of the brain is altered in sCJD, focusing instead on the spread of sCJD pathology along intact fibre projections. By seeding the model at all possible brain regions in turn, we show that the most likely seeds are also those that demonstrate the most dMRI abnormality. Specifically, we show that the top seed, in the posterior cingulate gyrus, recapitulates the spatial pattern of pathology observed on dMRI.

Our findings are concordant with a mechanism in which pathological prion species spread from a limited area of the brain along neural connections, ultimately producing a spatial pattern of disease governed by the structural connectome. Further investigation of top seed regions and associated neural connectivity pathways may prove to be a useful strategy for therapeutic development.

Materials and methods

Subject cohorts

MRI data were obtained from two publicly available subject cohorts. The first cohort is from Vitali *et al.* (2011), comprising 48 subjects from the University of California, San Francisco. There are 23 male subjects and 25 female subjects in this cohort, with a mean age of 63 years (range 40–81 years). The mean time from symptom onset to MRI scan was 8.5 months.

The second cohort is from Eisenmenger *et al.* (2016), comprising 37 subjects from the UK, who were referred to the National Prion Clinic. There are 23 male subjects and 14 female subjects in this cohort, with a mean age of 65 years (range 39–85 years). The mean time from symptom onset to MRI scan was 5.7 months.

Mapping of dMRI signal abnormalities

Average regional dMRI abnormalities were obtained from the datasets published in Vitali *et al.* and Eisenmenger *et al.* For Vitali *et al.*, diffusion-weighted imaging (either diffusion-weighted imaging with 3 diffusion-encoding directional gradients or diffusion tensor imaging with 6 or 15 directional gradients) was acquired at 1.5T on two

GE Signa scanners. The b value was 1000 s/mm^2 . Slice thickness varied from 3 to 5 mm. The mean diffusion in each region was visualized, and two neuroradiologists (with experience of 4 and 20 years) rated each region for the presence of abnormal hyperintensity, based on the extensive clinical knowledge of the normal appearance of the brain on clinical MRI. Each region was assigned a score of 0, 1 or 2 corresponding to the number of readers rating it as hyperintense.

For Eisenmenger *et al.*, diffusion-weighted imaging (either diffusion-weighted imaging with 3 diffusion-encoding directional gradients or diffusion tensor imaging with 64 directional gradients) was acquired on 1.5- or 3-T scanners including the GE Signa LX and Siemens TIM Trio. The b value was 1000 s/mm^2 . Slice thickness varied from 2 to 5 mm. Similar to Vitali *et al.*, each region was assigned a score of 0, 1 or 2 based on the appearance of the average regional diffusion, where 0 indicates normal, 1 indicates mild hyperintensity and 2 indicates clear hyperintensity; white matter was also used as an internal reference standard.

For the purposes of this study, the scores from both studies were considered analogous with a regional score of 0 denoting normal, 1 denoting intermediate hyperintensity and 2 denoting marked hyperintensity.

To facilitate joint analysis with the structural connectome, regional dMRI abnormality scores were mapped from the original 62 region atlases in each study to corresponding areas of the Desikan–Killiany atlas (Desikan *et al.*, 2006), filling 66 out of 86 possible regions. Semantic matching was used as the initial mapping strategy for each region (i.e. ‘caudate nucleus’ in the original 62-region atlas is mapped to ‘caudate nucleus’ in the Desikan atlas). For regions mapping to more than a single Desikan atlas region, the regional value was mapped to each of the relevant Desikan regions (for instance values for ‘hippocampus–amygdala’ are mapped to both ‘hippocampus’ and ‘amygdala’ in the Desikan atlas). Values for multiple regions mapping to a single Desikan region were averaged (for instance values for ‘thalamus anterolateral’ and ‘thalamus posteromedial’ were averaged and the average value mapped to ‘thalamus’ in the Desikan atlas).

Regional prevalence of dMRI signal abnormality is defined as the proportion of patients who demonstrate abnormal dMRI signal (i.e. score 1 or 2) for each region in each study.

Glassbrain representations of dMRI signal and prevalence, as well as all additional variables rendered in this way, display the variable of interest as a sphere centred within the region with radius proportional to the value.

Structural connectome

Axial T_1 -weighted structural fast spoiled gradient-echo scans (echo time = 1.5 ms, repetition time = 6.3 ms, inversion time = 400 ms, 15° flip angle, $230 \times 230 \times 156$

isotropic 1 mm voxels) and high angular resolution diffusion imaging data (55 directions, $b = 1000 \text{ s/mm}^2$, 72 1.8-mm-thick interleaved slices, $0.8594 \text{ mm} \times 0.8594 \text{ mm}$ planar resolution) were acquired on a 3-T GE Signa EXCITE scanner from 73 fully consented young healthy volunteers (40 men and 33 women, mean age 30 years) under a previous study approved by the Weill Cornell institutional review board; for details of study protocols, see Kuceyeski *et al.* (2013). Tractograms were extracted from these 73 young healthy subjects to create the normative connectome for the study. The measure of connectivity used here is the anatomical connection strength (Iturria-Medina *et al.*, 2008). The overall differences in regional connectivity were normalized by a scaling factor equal to the sum of the connections. Thus, the connection strength, $c_{i,j}$, between ROIs i and j , was defined as the anatomical connection strength score of streamlines connecting the two GM regions i and j . We refer to this network as graph $G = \{V, E\}$ whose nodes $v_i \in V$ represent the i th GM region, and edges $e_{i,j} \in E$ represent white matter fibre pathways whose connection strength is $c_{i,j}$. Connections are assumed to be bidirectional since directionality is not deducible from diffusion tensor imaging tractography data. A subset of the full connectome was created using only the values for the 66 GM regions mapped from the dMRI data.

Graph theoretical analysis of structural connectivity

Graph theoretical measures of degree centrality, betweenness centrality, eigenvector centrality and mean distance were computed using the Matlab implementation of the Brain Connectivity Toolbox (BCT; Rubinov and Sporns, 2010). The Pearson correlation coefficient r for regional dMRI signal abnormality and each regional graph theoretical measure of interest was computed. To assess whether significant correlations of regional dMRI signal abnormality with betweenness centrality and mean distance were due to underlying correlations with degree centrality, we created 10^3 random graphs from the connectivity matrix with preserved degree distribution using the Brain Connectivity Toolbox function ‘null_model_und_sign’ and then computed the Pearson correlation coefficient r for dMRI signal abnormality and the graph theoretical measure of interest. The mean of the resultant sampling distribution of r was then calculated.

Regional transcriptional analysis

The genes encoding prion protein (PRNP) and mGluR8 (GRM8) were identified for regional transcriptional analysis. For each gene, data were obtained from the publicly available human Allen Brain Atlas (ABA; Hawrylycz *et al.*, 2012). The ABA includes 926 brain regions, with each region having microarray expression levels from a set of 58 692 probes that correspond to 29,181 distinct

genes. ABA samples were mapped to the 66-region subset of the Desikan–Killiany atlas. All samples for all probes within the same region were then averaged for each gene. White matter tracts were excluded from analysis. Expression for each gene was averaged for six subject brains (which comprises data for six left hemispheres and two right hemispheres; more information can be found at help.brain-map.org/download/attachments/2818165/Normalization_WhitePaper.pdf).

Network diffusion modelling

sCJD disease progression is considered as a diffusion process on the connectivity matrix C , referred to as the network diffusion model (NDM) (Raj *et al.*, 2012). Briefly, the transmission of pathology from Region 1 to Region 2 is asserted to satisfy the equation $\frac{dx_1}{dt} = \beta c_{1,2}(x_2 - x_1)$, where x_1 and x_2 are pathology concentrations in the two regions and β is a global diffusivity constant empirically set to 0.15 (Pandya *et al.*, 2019). Extending this relationship to all regions i we define the regional pathology vector $\mathbf{x}(t) = \{x_i(t)\}$, and the above equation becomes, after appropriate normalization of the connectivity matrix by node degree, $\frac{d\mathbf{x}(t)}{dt} = -\beta H\mathbf{x}(t)$, where H is the graph Laplacian $H = I - D^{-\frac{1}{2}}CD^{-\frac{1}{2}}$.

The above linear differential equation has a closed-form solution, in which the regional pathology vector \mathbf{x} at timepoint t is given by the equation $\mathbf{x}(t) = e^{-\beta Ht}\mathbf{x}_0$ where \mathbf{x}_0 is the initial state of the model at $t=0$ (e.g. initial pathological insult). The NDM was separately initialized at all possible seed regions such that \mathbf{x}_0 is 1 at the seed region and 0 at all other regions. The Pearson correlation coefficient (R) of the actual measured dMRI signal abnormality map with the NDM-predicted regional pathology vector $\mathbf{x}(t)$ was calculated for each timepoint t and for each seed region. The maximum R occurring over all model timepoints t for each seed region was determined and is considered as a measure of seed region likelihood (SR). SR was also calculated for the top seed region best NDM prediction and 10^4 random permutations of the true dMRI map, yielding ‘SR_{scrambled}’.

Directional connectivity bias for the top seed region right posterior cingulate gyrus was simulated by varying the fraction of outgoing connections in the connectivity matrix C from 0.01 to 1 in increments of 0.01. SR was computed for each of the resultant directional models.

Following model initialization, we also calculate arrival time for each non-seed region, defined as the time t at which 98% of the maximum theoretical $x(t)$ value in that region is achieved.

Data availability

All data will be made available upon reasonable request.

Results

Stereotypical disease pattern across patient cohorts

Regional dMRI abnormalities have been reported for sCJD patient cohorts in Vitali *et al.* (2011) and Eisenmenger *et al.* (2016). Glassbrain representations of regional dMRI abnormality prevalence in these two studies are shown in Fig. 1A and B. The overall regional pattern of disease is similar in these two cohorts, with commonly affected areas including the cingulate gyrus, superior frontal gyrus and caudate nucleus. There is a substantial overlap in the top 20 most commonly affected regions, with 13 of the same regions represented in the top 20 for each cohort (Dice coefficient 0.65) (Fig. 1C). Regional prevalence is significantly correlated across cohorts ($r=0.59$, Fig. 1D), demonstrating that there is a stereotypical pattern of sCJD pathology despite significant heterogeneity within and across patient cohorts. There are some differences between the cohorts despite the similar overall pattern, which may be due in part to subject heterogeneity. The Vitali *et al.* cohort exhibits more widespread pronounced dMRI abnormalities, which may reflect a more advanced disease state, as the mean time of MRI scanning was 8.5 months from symptom onset versus 5.7 months in Eisenmenger *et al.*

Furthermore, the prevalence of dMRI signal abnormality is very highly correlated with the magnitude of the signal abnormality in the Eisenmenger cohort ($r=0.95$, Fig. 1D), suggesting that regions that are affected more commonly are also affected more severely by prion pathology.

Graph theoretical measures of regional connectivity predict dMRI signal

To investigate possible relationships between dMRI abnormalities and regional interconnectivity, we computed three different measures of network centrality as well as the mean number of connections required to reach the region of interest from another region (mean distance) (Fig. 2). Degree centrality and betweenness centrality are positively correlated with dMRI signal ($r=0.42$, $P=5.0 \times 10^{-4}$ and $r=0.34$, $P=5.6 \times 10^{-3}$, respectively), suggesting that highly affected regions have more connections and are located in more interregional pathways. The mean correlation of dMRI signal with random graph betweenness centrality is only 0.04 ($n=10^3$ random graphs), suggesting that the effect of betweenness centrality is not only due to the underlying degree structure of the structural connectivity matrix.

Eigenvector centrality is not correlated with dMRI signal ($r = -0.006$, $P=0.96$), suggesting that all

interregional connections are relevant, not just those to other highly connected regions. Mean distance (i.e. topological path length) is negatively correlated with dMRI signal ($r = -0.40$, $P=9.3 \times 10^{-4}$), possibly indicating that highly affected regions are those that can be reached from other regions via a fewer number of connections, on average. However, the mean correlation of dMRI signal with random graph mean distance is -0.42 , very similar to the value of -0.40 derived from the true connectivity matrix, suggesting that the underlying degree distribution of the connectivity matrix drives this effect. Together, these results suggest that highly affected regions are also those with connectivity properties well suited to receive and disseminate pathological prion species.

Regional expression of PRNP and genetic modifier GRM8 does not predict dMRI signal

Given that structural connectivity measures predict abnormality in microstructural integrity measured on dMRI, we sought to determine whether local genetic factors, which may be considered as surrogates of innate regional vulnerability to sCJD pathology, are also influential. To this end, we computed average regional transcript abundance from the ABA for PRNP (which encodes cellular prion protein) and GRM8 (which encodes the metabotropic glutamate receptor mGluR8), an sCJD GWAS genetic modifier (Sanchez-Juan *et al.*, 2015). We found that PRNP expression is not correlated with dMRI signal (Fig. 3A), suggesting that other factors are more important than PRNP transcript abundance in promoting regional pathology. Similarly, GRM8 expression (Fig. 3B) is uncorrelated with dMRI signal.

NDM predicts the spatial disease pattern from single seeds

We next asked whether the regional pathology pattern on dMRI can be predicted by NDM, which mathematically encapsulates the hypothesized mechanism of prion propagation along neural connectivity pathways. A schematic representation of the modelling approach is shown in Fig. 4A. Using this methodology, we find that the right posterior cingulate gyrus is the most likely seed region (seed region likelihood (SR) = 0.53, $P=5.4 \times 10^{-6}$). To assess whether the best fit NDM prediction is likely to achieve this level of correlation with the dMRI map by chance, we repeatedly randomly permuted the dMRI map vector and calculated the resultant SR (SR_{scrambled}) from the permuted dMRI map. We find that the mean SR_{scrambled} is ~ 0 (mean = 4.7×10^{-4} , standard deviation = 0.12) while the maximum SR_{scrambled} is 0.47, less than the true SR derived from the non-permuted dMRI map (Fig. 4B). This suggests that the high SR observed for the top seed region is

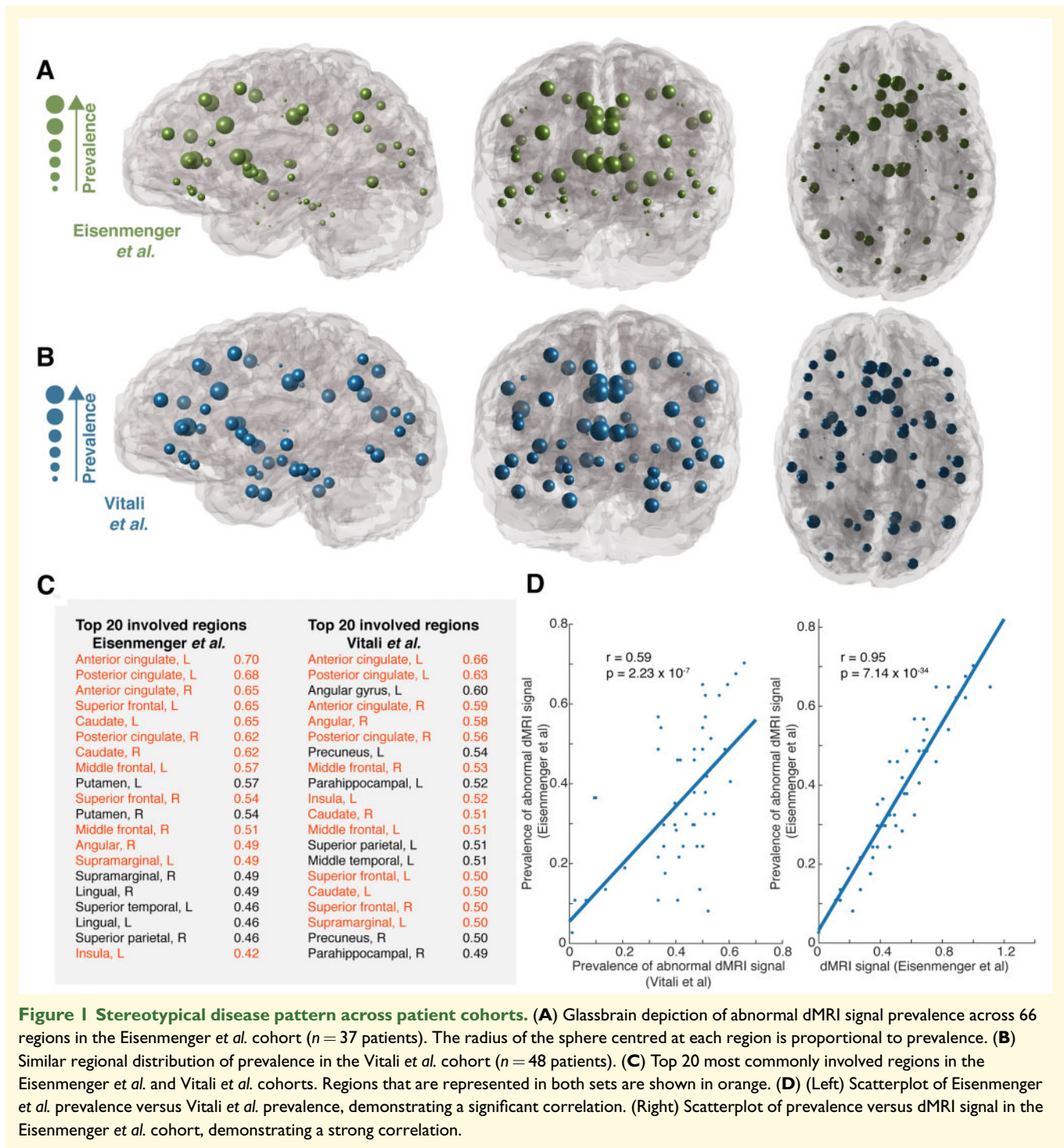


Figure 1 Stereotypical disease pattern across patient cohorts. **(A)** Glassbrain depiction of abnormal dMRI signal prevalence across 66 regions in the Eisenmenger et al. cohort ($n = 37$ patients). The radius of the sphere centred at each region is proportional to prevalence. **(B)** Similar regional distribution of prevalence in the Vitali et al. cohort ($n = 48$ patients). **(C)** Top 20 most commonly involved regions in the Eisenmenger et al. and Vitali et al. cohorts. Regions that are represented in both sets are shown in orange. **(D)** (Left) Scatterplot of Eisenmenger et al. prevalence versus Vitali et al. prevalence, demonstrating a significant correlation. (Right) Scatterplot of prevalence versus dMRI signal in the Eisenmenger et al. cohort, demonstrating a strong correlation.

unlikely to be due to chance similarity between the NDM prediction and dMRI map (true SR z -score derived from the $SR_{scrambled}$ distribution = 4.4, $P = 9.8 \times 10^{-6}$).

The next three top seed regions are also located within the cingulate gyrus (SR = 0.50–0.44), suggesting

that this region serves as a critical disease epicentre in controlling the regional pattern of disease. The remaining top 10 seed regions are listed in Fig. 4B. We find that dMRI signal and prevalence are highly correlated with SR (Fig. 4C), indicating that commonly and severely affected regions are those identified as

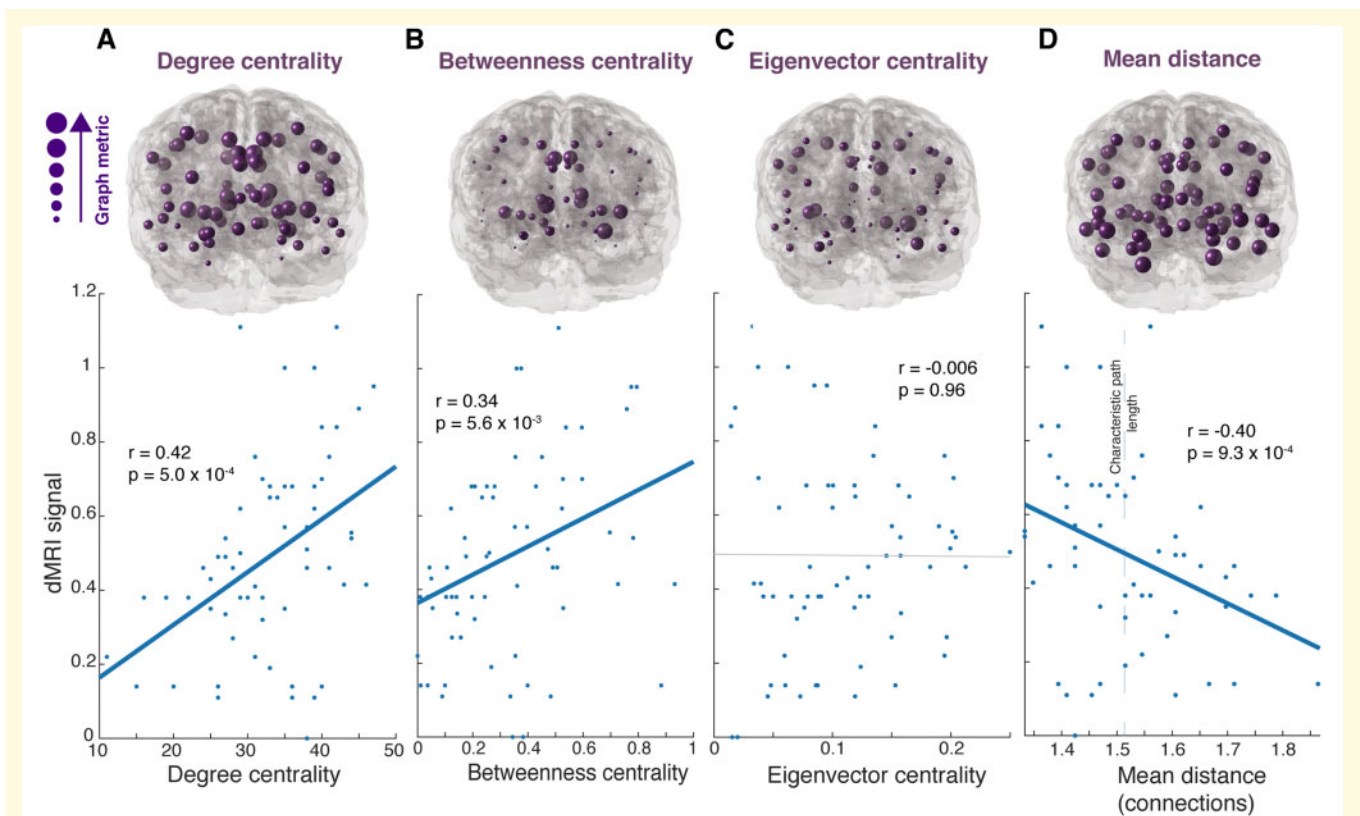


Figure 2 Graph theoretical measures of regional connectivity predict dMRI signal. Glassbrain representations of connectivity measures and scatterplots of each measure with dMRI signal. (A) Degree centrality and (B) betweenness centrality are positively correlated with dMRI signal. (C) Eigenvector centrality is not significantly correlated with dMRI signal. (D) Mean pathway distance to each region is negatively correlated with dMRI signal, but the correlation coefficient is similar to that derived from random graphs.

likely seed regions by our unbiased modelling methodology.

NDM prediction from the posterior cingulate recapitulates the spatial pattern of disease

We further investigated the spatial pattern of disease predicted from single model seeding at the right posterior cingulate gyrus. Visual inspection of the overall spatial pattern of dMRI abnormality predicted by NDM verifies close approximation to the measured dMRI abnormality map (Fig. 5A and B). Predicted dMRI abnormality is more conspicuous in the right hemisphere, reflecting unilateral seeding ($SR_{\text{Right}} = 0.55$, $P = 8.6 \times 10^{-4}$, $n = 33$ right-sided regions). However, a similar pattern of disease is evident in the left hemisphere with relatively smaller average dMRI abnormality ($SR_{\text{Left}} = 0.53$, $P = 1.5 \times 10^{-3}$, $n = 33$ left-sided regions). Seeding at the bilateral posterior cingulate gyrus improves SR only to 0.55 from 0.53 for unilateral seeding at the right posterior cingulate gyrus, indicating that bilateral seeding is not substantially more plausible than single region seeding.

We performed an additional simulation using an expanded connectome defined on the full 86-region Desikan–Killiany atlas to determine whether disease propagation in GM regions not assessed by dMRI could alter our results. We obtained similar findings with right anterior cingulate gyrus as the top seed region ($SR = 0.48$) and right posterior cingulate gyrus as the second ranked seed region ($SR = 0.44$). Left anterior and posterior cingulate gyri were the next ranked seeds ($SR = 0.43$ and 0.42 , respectively), again reinforcing an important role for cingulate gyrus in the disease process.

Simulated influence of directional connections on NDM prediction

We next asked whether the model is influenced by disproportionately directional connections to the top seed region since directional interregional connections are abundant in the brain, but largely inaccessible to empirical tractography (Leopold *et al.*, 2014). We performed NDM simulations seeded at the right posterior cingulate gyrus with fractional outgoing connection directionality from this region varying from 0.01 to 1 (Fig. 5D). As our results thus far have used a nondirectional

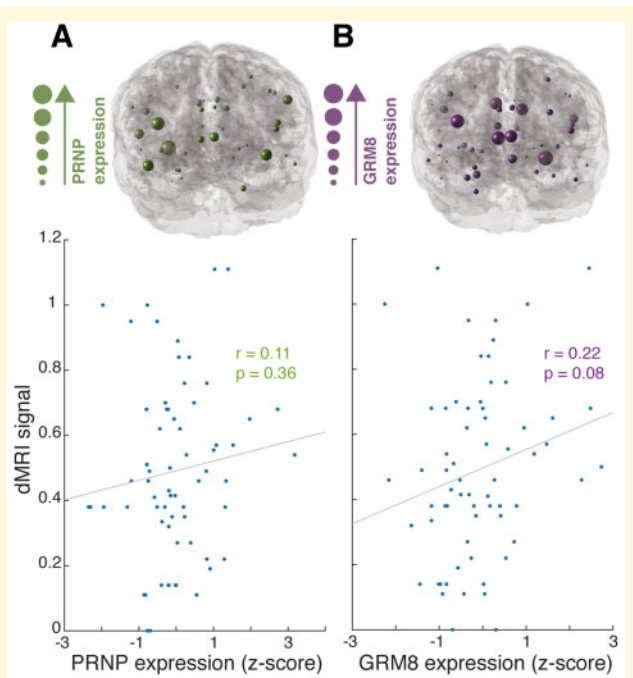


Figure 3 Regional expression of PRNP and genetic modifier GRM8 does not predict dMRI signal. (A) Glassbrain representation of PRNP regional transcript abundance and scatterplot with dMRI signal. There is no significant correlation between dMRI and PRNP expression. (B) Glassbrain representation of GRM8 regional transcript abundance and scatterplot with dMRI signal. There is no significant correlation between dMRI and GRM8 expression.

connectome (fractional outgoing connections = 0.5), we sought to determine whether model fit could be improved or degraded by varying directional connectivity bias from the top seed region, right posterior cingulate gyrus. We find that increasing retrograde connection bias improved model fit from the nondirectional model with SR approaching 0.6. In contrast, increasing anterograde bias degraded model fit significantly with SR approaching 0.2 with purely outgoing connections arising from the top seed. However, we do note that model fit degradation is probably more sensitive to increasing outgoing connection strength, as outgoing connections influence the model trajectory immediately in its timecourse. Incoming connections must exert their influence after seeded pathology has been transmitted to another region and back to the top seed, forming a loop.

NDM temporal spread predicts regional dMRI prevalence

We next asked whether the prevalence of dMRI signal abnormality can be predicted by the NDM temporal pattern of disease evolution. To this end, we quantify NDM ‘arrival time’, defined as the model timepoint at which a given region achieves 98% of its maximal dMRI signal

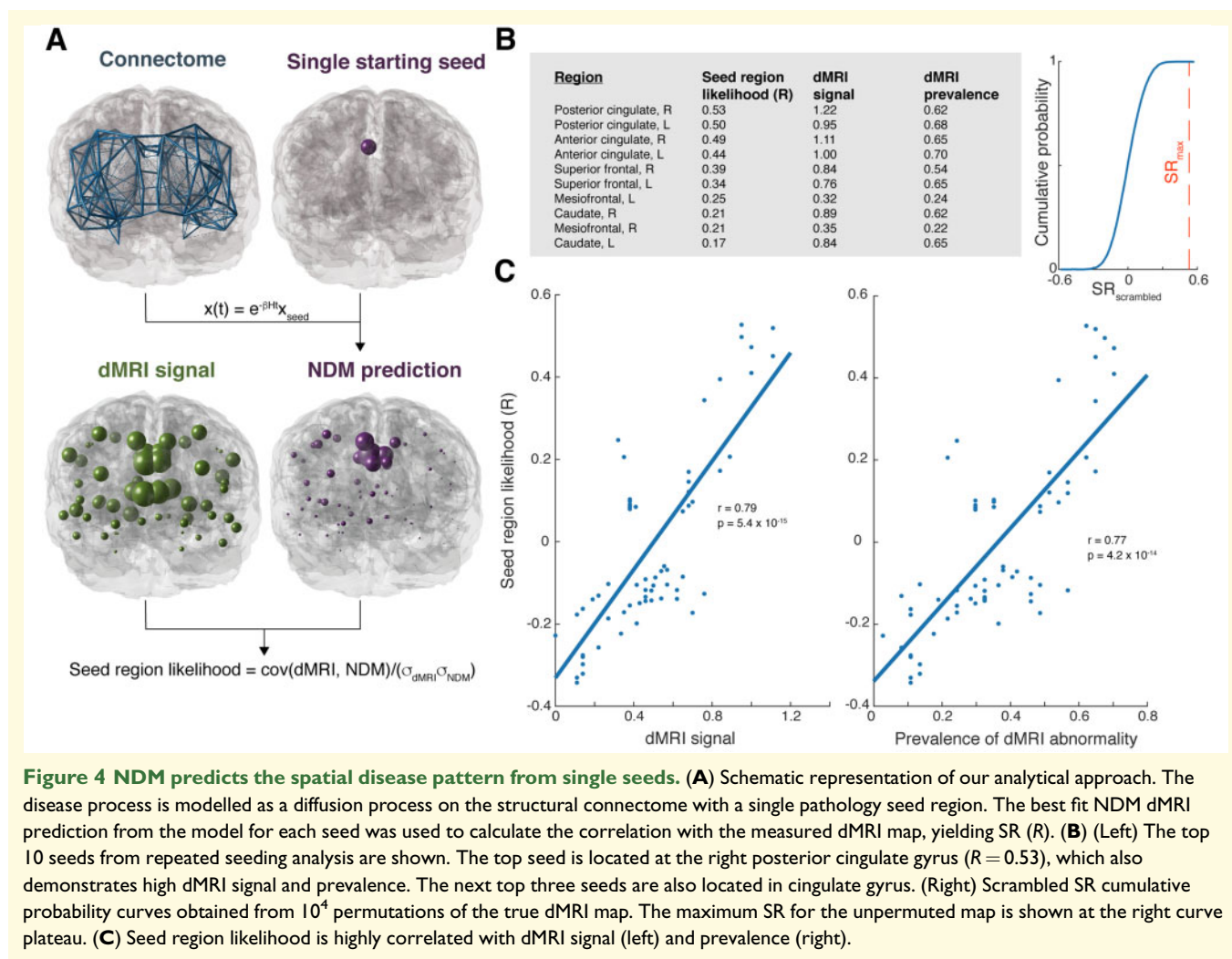
abnormality following seeding at the right posterior cingulate gyrus. In this context, regions with smaller arrival times are those that are affected earlier due to misfolded prion propagation from the top seed region. We find that prevalence correlates negatively with arrival time ($r = -0.47$), suggesting that regions affected earlier in the disease process more commonly exhibit dMRI abnormalities.

Discussion

Here, we demonstrate that the regional pattern of sCJD pathology on neuroimaging can be substantially explained by a network spread process originating in a single brain region. Using graph theoretical analysis of the structural connectome, we show that highly affected brain regions are also highly connected to other brain regions. Top seed regions such as the posterior cingulate gyrus are thereby optimally positioned to serve as both accumulators and propagators of prion pathology via interregional connections. Previous graph theoretic studies of other dementias have reported the existence of such disease ‘epicentres’, which may anchor diverse proteinopathies (Seeley et al., 2009; Zhou et al., 2012).

While a graph theoretical framework has been employed to gain insight into various forms of neurodegenerative disorders (Raj et al., 2012; Mezas et al., 2020), trauma (Caeyenberghs et al., 2012) and ischaemia (Crofts et al., 2011), we are not aware of any prior studies utilizing this approach in prion disorders. The proposed molecular mechanism of prion disease pathogenesis and intercellular spread is effectively translated to the macroscopic scale using our graph theoretical and NDM approach. Indeed, here, we show for the first time that macroscopic features of sCJD visible on neuroimaging can be explained by interregional structural connectivity and accurately modelled by assuming that disease propagation from a single region can explain the global pattern of pathology. Our results are compatible with a scenario in which a single misfolded prion could cause a devastating cascade of pathology that involves numerous brain regions.

These findings are particularly important in light of recent work on the trans-neuronal spread of tau in Alzheimer’s disease, as they provide strong verification of this mechanism using human imaging data in the canonical trans-neuronal disease process. For example, Franzmeier et al. (2019) recently showed an association between functionally connected regions and the regional burden of tau as assessed by PET. The same group recently extended these findings to show that regional increases in tau over time are predicted by changes in connected brain areas (Franzmeier et al., 2020). Similar to the findings in our study, strongly connected regions were found to be particularly susceptible to tau accumulation (Cope et al., 2018; Hoenig et al., 2018), suggesting



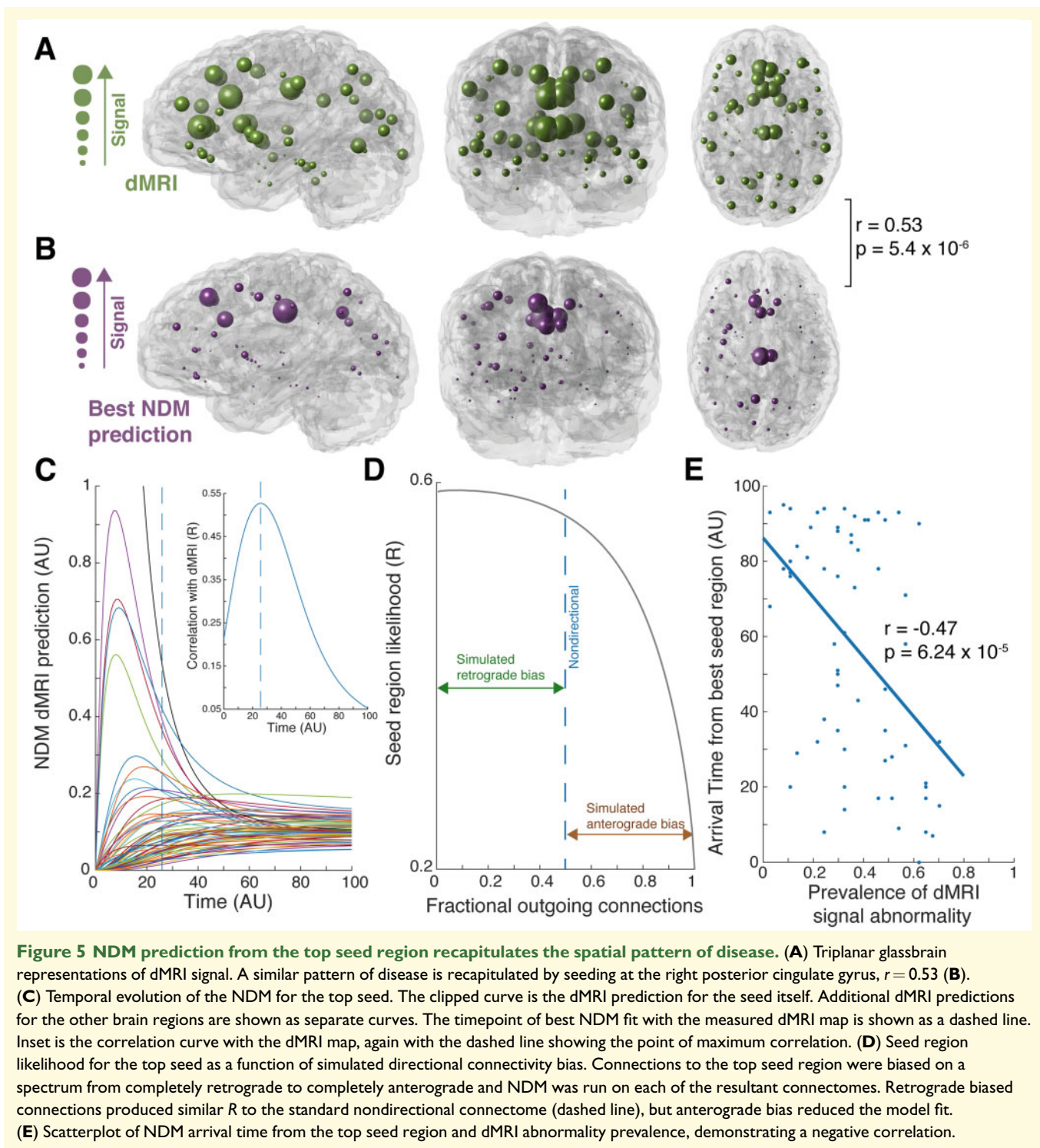
that such regions may serve as critical accumulators and disseminators of pathological proteins.

Furthermore, the predictive accuracy of our NDM results are on par with those cited in other recent studies of Alzheimer's disease (Acosta *et al.*, 2018) and Parkinson's disease (Pandya *et al.*, 2019), despite the use of much larger patient cohorts and fully quantitative MRI target measures of pathology in these studies. This may indicate that NDM may offer even more powerful predictive capacity in future studies that utilize single subject data, CJD-specific structural connectivity or more quantitative measures of dMRI abnormalities.

The central role of the cingulate gyrus in sCJD is intriguing. We note that the top seed region, the right posterior cingulate gyrus is (along with the left posterior cingulate gyrus) the most highly connected region in our 66 region brain parcellation as measured by degree centrality. Three of the four regions with the largest connection strengths to this region are also top seed regions—the left posterior cingulate gyrus, right anterior cingulate gyrus and right superior frontal gyrus. These areas likely

comprise a core network within the brain that accumulates prion pathology and promotes its spread within and beyond the network in the early disease state.

Our modelling approach is compatible with known features of prion pathology at the mesoscopic and microscopic levels. We find that the regional pathology pattern can be predicted using only a single brain region as a pathology seed. This is in accordance with the hypothesis that a single misfolded prion could initiate mass conversion of normal species by corruptive templating. Evidence showing that prions can be transmitted along neural connectivity pathways is also compatible with our model. We find a likely role for both retrograde and anterograde connections from the top seed region posterior cingulate gyrus, in accordance with biochemical data demonstrating that prion-containing vesicles can undergo both anterograde and retrograde axonal transport via kinesin- and dynein-dependent mechanisms (Encalada *et al.*, 2011). However, incoming connections seem particularly important as simulating an increase in the fraction of incoming connections improves model fit. This may suggest that the



posterior cingulate gyrus assumes a prominent role in the disease process by aggregating misfolded prions from diverse connected brain regions.

We do not find a role for the regional transcription of PRNP or GRM8 in predicting seed location. While transcript levels are informative, they are less relevant to cellular function than protein levels and function. In this case, there may be more important cellular factors that

lead to prion misfolding and accumulation than regional variation in transcription. However, we note that data from the ABA come from healthy normal subjects and it is possible that subjects with risk factors for developing sCJD may have differing transcriptional profiles that influence disease pathogenesis. In the future, transcriptomic and proteomic analyses of sCJD subjects may provide further insight into this issue.

There are several limitations to our study that warrant discussion. The first is that regional dMRI signal in both datasets utilized here are described with a simple 3-tier scoring scheme. While this may prove useful for clinical imaging applications and promotes inter-reader reliability for neuroradiologists, it necessarily introduces compression of the dMRI dataset, and loss of potentially useful information. Direct quantification of apparent diffusion coefficient is an alternative consideration, but there are also limitations to this approach including variability across MRI scanners and magnetic field strengths. For instance, a study directly quantifying apparent diffusion coefficient (Caverzasi *et al.*, 2014) noted several discrepancies between the findings using this approach and those more firmly established by expert reader visual analysis, possibly due to technical factors.

A second limitation is the relatively small number of subjects. This is partially an inherent limitation of studying a rare disease. Nonetheless, these datasets are limited by the signal-to-noise ratio of dMRI and decreased power in statistical hypothesis testing. Despite these limitations, the robust effects we find here suggest that there is a powerful mechanistic basis underlying the stereotypical pattern of disease observed on MRI. Future work investigating disease progression in individual subjects may provide further insight into the disease process. For instance, while we find that right posterior cingulate gyrus is the top seed region, it is likely that some subjects tend to exhibit more disease in the corresponding contralateral region. Examining these differences in individual subjects may improve prediction accuracy and reveal important subgroups with prognostic or therapeutic implications.

A third limitation is that we have necessarily employed a normative connectome derived from young healthy subjects instead of CJD subjects, due to the lack of sufficient multidirectional dMRI data from the CJD subject cohorts. While using a CJD-specific connectome would be ideal, there are reasons why using a normative connectome is reasonable in its absence. The first is that there is no published evidence of a gross difference in overall structural brain network topology between healthy people and CJD patients. The second is that a recent study of NDM in Alzheimer's disease demonstrated that NDM predictions were not significantly different when using an AD-specific connectome or the young healthy normative connectome (Powell *et al.*, 2018). We hope to address this question for CJD in the future as more data become available.

An additional issue is that while NDM provides accurate predictions of the regional dMRI map based on macroscopic structural connectivity, there are likely additional factors that control regional sensitivity to prion pathology that our model does not include. For instance, we find that NDM underestimates the dMRI signal in the caudate nuclei. This may reflect region-specific cellular factors that render this area particularly sensitive to prion pathology, apart from its position in the structural

connectivity network. In the mouse brain, it has been shown that there are specific regional distributions of different cellular prion protein isoforms (Beringue *et al.*, 2003), which may influence conformation conversion rates and susceptibility to PrP^{Sc}-induced pathology. Accordingly, analogous isoform distributions in humans may in part explain disease patterning.

In summary, intrinsic properties of the structural brain network can largely explain the regional pattern of sCJD disease observed on MRI. Further investigation of top seed regions and associated connectivity pathways may provide insight into the early disease state and potential therapeutic interventions. A more extensive understanding of pathology patterning in sCJD may also inform future studies of other diseases, which also likely involve trans-neuronal spread of pathological proteins, such as Alzheimer's disease and Parkinson's disease.

Funding

A.R. and S.P. were supported by National Institutes of Health (NIH) grants RO1NS092802 and R01AG062196. A.R. was also supported by National Institutes of Health (NIH) grant R56AG064873.

Competing interests

No competing interests or financial disclosures.

References

- Acosta D, Powell F, Zhao Y, Raj A. Regional vulnerability in Alzheimer's disease: the role of cell-autonomous and transneuronal processes. *Alzheimers Dement* 2018; 14: 797–810.
- Bartz JC, Kincaid AE, Bessen RA. Rapid prion neuroinvasion following tongue infection. *J Virol* 2003; 77: 583–91.
- Beringue V, Mallinson G, Kaiser M, Tayebi M, Sattar Z, Jackson G, et al. Regional heterogeneity of cellular prion protein isoforms in the mouse brain. *Brain* 2003; 126: 2065–73.
- Caeyenberghs K, Leemans A, Heitger MH, Leunissen I, Dhollander T, Sunaert S, et al. Graph analysis of functional brain networks for cognitive control of action in traumatic brain injury. *Brain* 2012; 135: 1293–307.
- Caverzasi E, Henry RG, Vitali P, Lobach IV, Kornak J, Bastianello S, et al. Application of quantitative DTI metrics in sporadic CJD. *NeuroImage Clin* 2014; 4: 426–35.
- Cope TE, Rittman T, Borchert RJ, Jones PS, Vatansever D, Allinson K, et al. Tau burden and the functional connectome in Alzheimer's disease and progressive supranuclear palsy. *Brain* 2018; 141: 550–67.
- Crofts JJ, Higham DJ, Bosnell R, Jbabdi S, Matthews PM, Behrens TEJ, et al. Network analysis detects changes in the contralesional hemisphere following stroke. *Neuroimage* 2011; 54: 161–9.
- Desikan RS, Ségonne F, Fischl B, Quinn BT, Dickerson BC, Blacker D, et al. An automated labeling system for subdividing the human cerebral cortex on MRI scans into gyral based regions of interest. *Neuroimage* 2006; 31: 968–80.
- Eisenmenger L, Porter M-C, Carswell CJ, Thompson A, Mead S, Rudge P, et al. Evolution of diffusion-weighted magnetic resonance

- imaging signal abnormality in sporadic Creutzfeldt–Jakob disease, with histopathological correlation. *JAMA Neurol* 2016; 73: 76–84.
- Encalada SE, Szpankowski L, Xia C, Goldstein LSB. Stable kinesin and dynein assemblies drive the axonal transport of mammalian prion protein vesicles. *Cell* 2011; 144: 551–65.
- Franzmeier N, Neitzel J, Rubinski A, Smith R, Strandberg O, Ossenkoppele R, et al.; Alzheimer’s Disease Neuroimaging Initiative (ADNI). Functional brain architecture is associated with the rate of tau accumulation in Alzheimer’s disease. *Nat Commun* 2020; 11: 347.
- Franzmeier N, Rubinski A, Neitzel J, Kim Y, Damm A, Na DL et al.; for the Alzheimer’s Disease Neuroimaging Initiative. Functional connectivity associated with tau levels in ageing, Alzheimer’s, and small vessel disease. *Brain* 2019; 142: 1093–107.
- Fraser H. Neuronal spread of scrapie agent and targeting of lesions within the retino-tectal pathway. *Nature* 1982; 295: 149–50.
- Hawrylycz MJ, Lein ES, Guillozet-Bongaarts AL, Shen EH, Ng L, Miller JA, et al. An anatomically comprehensive atlas of the adult human brain transcriptome. *Nature* 2012; 489: 391–9.
- Hoening MC, Bischof GN, Seemiller J, Hammes J, Kukolja J, Onur ÖA, et al. Networks of tau distribution in Alzheimer’s disease. *Brain* 2018; 141: 568–81.
- Iturria-Medina Y, Sotero RC, Canales-Rodríguez EJ, Alemán-Gómez Y, Melie-García L. Studying the human brain anatomical network via diffusion-weighted MRI and Graph Theory. *Neuroimage* 2008; 40: 1064–76.
- Kuceyeski A, Maruta J, Relkin N, Raj A. The Network Modification (NeMo) tool: elucidating the effect of white matter integrity changes on cortical and subcortical structural connectivity. *Brain Connect* 2013; 3: 451–63.
- Leopold DA, Modi P, Thomas C, Irfanoglu MO, Saleem KS, Ye FQ, et al. Anatomical accuracy of brain connections derived from diffusion MRI tractography is inherently limited. *Proc Natl Acad Sci USA* 2014; 111: 16574–9.
- Manners DN, Parchi P, Tonon C, Capellari S, Strammiello R, Testa C, et al. Pathologic correlates of diffusion MRI changes in Creutzfeldt–Jakob disease. *Neurology* 2009; 72: 1425–31.
- Mezias C, Rey N, Brundin P, Raj A. Neural connectivity predicts spreading of alpha-synuclein pathology in fibril-injected mouse models: Involvement of retrograde and anterograde axonal propagation. *Neurobiol Dis* 2020; 134: 104623.
- Pan KM, Baldwin M, Nguyen J, Gasset M, Serban A, Groth D, et al. Conversion of alpha-helices into beta-sheets features in the formation of the scrapie prion proteins. *Proc Natl Acad Sci USA* 1993; 90: 10962–6.
- Pandya S, Zeighami Y, Freeze B, Dadar M, Collins DL, Dagher A, et al. Predictive model of spread of Parkinson’s pathology using network diffusion. *Neuroimage* 2019; 192: 178–94.
- Powell F, Tosun D, Sadeghi R, Weiner M, Raj A; Alzheimer’s Disease Neuroimaging Initiative. Preserved structural network organization mediates pathology spread in Alzheimer’s Disease spectrum despite loss of white matter tract integrity. *J Alzheimers Dis* 2018; 65: 747–64.
- Raj A, Kuceyeski A, Weiner M. A network diffusion model of disease progression in dementia. *Neuron* 2012; 73: 1204–15.
- Rubinov M, Sporns O. Complex network measures of brain connectivity: uses and interpretations. *Neuroimage* 2010; 52: 1059–69.
- Sanchez-Juan P, Bishop MT, Kovacs GG, Calero M, Aulchenko YS, Ladogana A, et al. A genome wide association study links glutamate receptor pathway to sporadic Creutzfeldt–Jakob disease risk. *PLoS One* 2015; 10: e0123654.
- Seeley WW, Crawford RK, Zhou J, Miller BL, Greicius MD. Neurodegenerative diseases target large-scale human brain networks. *Neuron* 2009; 62: 42–52.
- Shiga Y, Miyazawa K, Sato S, Fukushima R, Shibuya S, Sato Y, et al. Diffusion-weighted MRI abnormalities as an early diagnostic marker for Creutzfeldt–Jakob disease. *Neurology* 2004; 63: 443–9.
- Vitali P, Maccagnano E, Caverzasi E, Henry RG, Haman A, Torres-Chae C, et al. Diffusion-weighted MRI hyperintensity patterns differentiate CJD from other rapid dementias. *Neurology* 2011; 76: 1711–9.
- Young GS, Geschwind MD, Fischbein NJ, Martindale JL, Henry RG, Liu S, et al. Diffusion-weighted and fluid-attenuated inversion recovery imaging in Creutzfeldt–Jakob disease: high sensitivity and specificity for diagnosis. *Am J Neuroradiol* 2005; 26: 1551–62.
- Zerr I, Kallenberg K, Summers DM, Romero C, Taratuto A, Heinemann U, et al. Updated clinical diagnostic criteria for sporadic Creutzfeldt–Jakob disease. *Brain* 2009; 132: 2659–68.
- Zhou J, Gennatas ED, Kramer JH, Miller BL, Seeley WW. Predicting regional neurodegeneration from the healthy brain functional connectome. *Neuron* 2012; 73: 1216–27.